https://doi.org/10.1016/j.jclepro.2020.123433

Utilizing concrete pillars as an environmental mining practice in underground mines

Shuai Cao [1, 2, 3], Gaili Xue [1, 2], Erol Yilmaz [4, *], Zhenyu Yin [3], Fudou Yang [1, 2, 5]

[1] *State Key Laboratory of High-Efficient Mining and Safety of Metal Mines of Ministry of Education, Beijing 100083, China*

[2] *School of Civil and Resources Engineering, University of Science and Technology Beijing, Beijing 100083, China*

[3] *Department of Civil and Environmental Engineering, The Hong Kong Polytechnic University, Hung Hom, Kowloon, Hong Kong, China*

[4] *Department of Civil Engineering, Geotechnical Division, Recep Tayyip Erdogan University, Fener, Rize TR53100, Turkey*

[5] *Zijin Tungsten Industry Group Company Limited, Yunnan 8161003 China*

* Corresponding author.: erol.yilmaz@erdogan.edu.tr (E. Yilmaz)

E-mails: sandy_cao@ustb.edu.cn (S. Cao); hnpyxgl@126.com (GL. Xue); zhenyu.yin@polyu.edu.hk (ZY. Yin)

Abstract: Ground control is an integral element of mine design and worker safety. The use of concrete pillars for underground mines is of paramount importance to maintaining the economic and operational security of structures. This paper deals with the use of fiber-reinforced concrete (FRC) as pillars via laboratory and field tests. The strength performance of prepared concrete reinforced with glass, polypropylene and polyacrylonitrile fibers was researched by a mechanical press and a computed tomography (CT) tool. Samples were tested for fiber volume fractions of 0, 0.4, 0.8 and 1.2 wt.%, respectively. Results have indicated that, with the addition of fibers, the strength was improved first due to a bridging effect and then decreased due to a pull-out effect. Compared to the reference sample, the absorbed energy prevents FRC from deterioration by mechanisms of matrix cracking, fiber-matrix interface debonding and fiber rupture. The peak strains of FRC linearly rise with increasing fiber. The gray value distribution curves have also good correspondence with 2D CT pore and crack distributions, which reveal that gray value processing could depict the structural behavior of concretes reinforced with or without fiber. Theoretical analyses show that the pillar remains stable for sustainable mining. Besides, the location and size of FRC pillars are suitable for numerical calculations of the trial stope. The findings of this study can offer a key reference for the orebody pillar recovery in underground mines.

Keywords: Environmental mining practice; ore pillar recovery; fiber reinforced concrete; compressive strength; computed tomography; numerical simulation

Nomenclature

FRC	Fiber reinforced concrete	PAN	Polyacrylonitrile
CT	Computed tomography	FC	Fiber content
UCS	Uniaxial compressive strength	NFRC	None-fiber reinforced concrete
2D	Two-dimensional	NDT	None-destructive testing
3D	Three-dimensional	PS	Peak strain
NM	Nanwenhe mine	MCC	Multiple correlation coefficient
CMS	Cavity monitoring system	AEM	Average elastic modulus
PP	Polypropylene	C-S-H	Calcium-silicate-hydrate
C-H	Calcium hydroxide	AHP	Artificial hydraulic prop
F_s	Safety factor of orebody pillar	σ_c	Uniaxial compressive strength
γ	Density of overburden rock mass	H	Buried depth of the pillar
W	Width of the pillar	h	Height of the pillar
S_v	Section area of the Voronoi diagram	S_p	Section area of the pillar
Q	Economic value of pillar mining	T	Weight of orebody in trial stope
G_K	Average grade of orebody	R_X	Orebody mineral processing rate
R_c	Mining recovery rate	G_J	Grade of tungsten powder
P	Price of tungsten powder	C	Mining unit price
D	Cost of FRC pillars		

1 Introduction

Ground control problems in mines are linked to a high-stress environment (e.g., high extraction rates, high field ground stresses and deep mining) and the presence of several geological features. To manage the resulting induced stresses, mines consider different mining methods including pillars (Dong et al. 2019). To remove stress-related ground problems, the room-and-pillar method is used in flat-bedded deposits of limited thickness, such as coal, salt, limestone, gold and copper (Napa-García et al., 2019). This method is used to safely recover orebody in the open stope, and pillars were left to capably support the hanging-wall (Malli et al., 2017). Although the remaining pillars improved the stope stability, the loss of many pillars leads to enormous waste of the precious mineral resources (Esterhuizen et al., 2011). Judging the stability of the pillar is of great value to pillar recoveries and sustainable mining (Sherizadeh and Kulatilake, 2016). Researchers and engineers often use empirical methods, theoretical calculations and numerical simulation methods for suitably assessing the pillar stability (Tesarik et al., 2009; Yilmaz et al., 2013). Qiu et al. (2020) have recently proposed a new concept of recycling which will contribute to the industrialization of metallic resources recycle and energy saving. Consequently, both local and regional stability of underground mining structures should be well addressed in the in-situ conditions through an appropriate pillar design (Renani et al., 2018).

To safely extract the ore, numerous openings are inevitably generated during the underground mining process. These openings are typically 20 to 90 m high and 15 m × 15 m in-plane dimension, which often induce ground surface subsidence (Li et al., 2020) or mine collapse (Yin et al., 2020) unless the backfill is employed to better support the earlier-excavated openings. Besides, massive ore pillars that are left for supporting mining regions would cause enormous loss of mineral resources (Xue et al., 2019a). To provide additional structural support for continuous excavations and minimize the loss of minerals, the backfill is frequently used as either temporary or permanent pillars (Jiang et al., 2020). Using different underground mining methods, pillar recovery is done in different ways. Li et al. (2018) advance an artificial expandable pillar (formed by an engineered mix that expands when water is mixed) for underground pillar mining. It is found that expandable pillars can stabilize an excavation with small roof deformation. Waclawik et al. (2017) indicated that the rock bolting technique could well control the roof deformation in the room-and-pillar technique in the upper Silesian coal basin. Yu et al. (2018) considered the progressive pillar size reduction and the confining behaviors of coal debris and proposed an improved technique for the long-term stability evaluation of strip mining and pillar. Sun et al. (2018) adopted the cemented backfill system to mine coal pillar based on Qishan coal mine located in China. Hauquin et al. (2016) found a more accurate analytical technique to calculate vertical stresses on pillars of irregular size by using a finite code, which offered a better approximation than the existing methods. Ghasemi et al. (2014) shown that there is a clear relationship between pillar size and five parameters (e.g., depth of cover, mine height, panel width, roof strength and loading conditions), concluding that the most effective parameter on pillar size was loading conditions.

Indeed, when the room-and-pillar technique is employed for underground mining, the large blocks of ores in pillar form are mainly left in place to better support the mass of the neighboring rocks (Ghasemi et al., 2010). Unless these pillars are subsequently recovered, the ore deposits they contain will never be mined (Deng et al., 2019). Hence, pillar and its overall durability during the life of mine offer a key part for sustainable mine operations since pillars serve as a major ground support element for structures and offer a safe working platform for mine workers (Li et al., 2013). The final design of pillars can seriously affect the success of underground operations (Laurence, 2011). To safely extract ore pillars, which can produce high risks such as incidents and casualties, various techniques have been recently implemented in mines (Seccatore et al., 2014; Lu et al., 2020). One of these emerging techniques is to employ fiber reinforced concrete (FRC), which can reduce the formation of cracking, rise the composite absorption of energy, and improve the long-term tensile and compressive strength (Bdulkareem et al., 2019; Chan et al., 2019).

The artificial concrete pillar replacement method is an efficient technique to recovery orebody pillars. The feasibility of using different waste materials in recycled FRC attracts practitioners' attention (Merli et al., 2020). Some researchers have been done on the strength properties of concrete (Signorini et al., 2020; Feo et al., 2020). Laboratory testing and numerical simulations are the two main ways to develop the mechanical properties of concrete, soil and other polymeric materials (Emeka et al., 2018; Xiong et al., 2019). Usman et al. (2020) found that the use of steel fiber had a minute effect on the compressive strength of concrete, whereas it pointedly improved its ductility and enhanced its post-peak behavior. Qin et al. (2019) found that the addition of waste fiber could improve the compressive strength value of concrete. The fracture morphology and scanning electron microscope analyses showed the positive function of rubber aggregates and polypropylene fibers on post-crack propagation (Wang et al., 2020). The different types of additives such as rubber, steel, glass and polypropylene fibers were added into concrete to improve the strength and toughness (Liu et al., 2019). Salim et al. (2019) explored that the bond strength between the reactive powder concrete with glass fiber as a repair material and the normal strength concrete as a substrate layer is relatively high when compared to the concrete having steel and polypropylene fibers. Kadam et al. (2019) found that increasing the percentage of fiber volume, the compressive and flexural strength also increases. Moreover, carbon fiber plays an imperative role in improving the asphalt mixtures or other kinds of composites (Mawat and Ismael, 2020). The shearing tests found that the stiffness appeared more pronounced in the FRC panels than in the reference panel without fibers (Facconi et al., 2020). The addition of rubber powder improves the damping capacity of polypropylene-FRC while reducing the concrete strength and increasing the peak strain (Mo et al., 2020). The concrete mix reinforced with recycled polymer fiber also exhibited better flexural strength than that without fiber (Chen et al., 2020). The post-fracture behavior of macro polypropylene rubber FRC was improved with increasing residual load capacity and deformation (Wang et al., 2019).

The fiber reinforcement is presently being used in civil and geotechnical engineering. New types of fibers like polypropylene have been developed for FRC, soils, clays and gravels. One can report that the addition of fibers helps rectify the weakness of ordinary concrete by mobilizing tensile strength along the failure planes (Buttignol et al., 2020), and provided a crack-arresting ability and enhanced the strength (e.g., compressive, flexural, tensile and impact strengths), toughness and ductility (Grzymski et al., 2019). Polypropylene fibers have advantages of resistance to corrosion and easier dispersion within a concrete mix than steel fibers (Aarthi and Arunachalam, 2018; Koohestani et al., 2019). Similar test results from studies of fiber-reinforced sand and cemented soil are reported as well. The addition of randomly mixed fibers vividly increased the strength and stiffness of sand and soil as well as increased the shear strength without samples exhibiting distinct failure planes (Consoli et al., 2017). FRC is very popular in civil engineering, being used to increase the tensile and flexural strength of structures. In ordinary concrete, the internal micro-cracks contribute to the failure of structures and associated poor ductility (Alp et al., 2009; Hesami et al., 2016).

The above scientific works offer substantial information and technical data for better understanding of the strength characteristics of concrete and FRC. However, no research has been so far conducted on the laboratory and in-situ assessment of concrete pillars used as a support tool for quite a range of under different conditions such as sill pillar recovery, reduction of large stope spans and support of large size wedges. An in-depth understanding of the internal crack mechanism (through sliced images acquired from X-ray CT) and failure modes of FRC containing different fiber types and rates is critical for assessing their mechanical strength performance. This study presents the results of laboratory and field investigations of FRC to be used in the preliminary ground support design specifications of mines. A case study is also presented to better evaluate the in-situ behavior of FRC mass as a pillar, exhibiting structural behavior and integrity of FRC, which is related to rigidity, stiffness and strength. Additionally, the cavity monitoring system (CMS) scanning system was used for scanning the actual 3D shape of the mined-out areas and orebody pillars. The 3D geological software was then used for numerical modeling.

After this process, the geological model was introduced into the numerical simulation software to quantitatively assess the stability of pillars before and after mining. The Voronoi diagram was used to calculate the safety factors of pillars. The main goals of this study are: i) to assess the feasibility of FRC as a major ground support in underground mines; ii) to broadly analyze its internal structure by 3D reconstruction technology; iii) to assess the relationship between compressive strength and internal structure of FRC; iii) to understand the failure modes and structural characteristics of FRC, and to carry out on-site pillar mining application to better assess its applicability in real underground mine conditions.

In section 1, a literature review is given initially. The materials and methods including background and mining method plan, experimental materials, specimen preparation and test protocols are explained in section 2. The results and discussion including the mechanical properties of FRC, pillar mining on-site are presented in section 3. Finally, the conclusions are summarized, indicating the future works.

2 Materials and methods

2.1 Engineering background and mining method

Considering that underground mineral reserves will be depleted and less costly systems instead of orebody pillars, artificial concrete pillars can undoubtedly find a ground for economic and sustainable mining (Kaliyavaradhan et al., 2020). Nowadays, most mines are seriously addressing and examining all kinds of possibilities to drive down costs and run an effective operation (Dong et al., 2019). In this view, using artificial concrete pillars instead of natural orebody pillars can bring a solution to mines for improving the profitability of their mining operations (Xu et al., 2019). A case study presented in this study is just an example. There are lots of remaining pillars to be considered in underground mines. The room-and-pillar mining method was widely used in the 1970s because of its low production cost in Chinese gold and tungsten mines (Zingano and Weiss, 2019). The reason why numerous mines choose this method is closely related to the current price of the mined metal products. Nevertheless, with the increase in orebody price and the rapid consumption of mineral resources, the remaining pillars can be well considered for sustainable mining operations (Botín and Vergara, 2015). There are still many underground mines using this method around the world. The appropriate pillar mining method can also bring wide application prospects (Waclawik et al., 2017).

The NM, which is located in the Yunnan province of China, owned and operated by Zijin Mining Group Company Limited founded in 2007. The mine uses the room-and-pillar mining method to exploit the orebody. Each stope is divided into 80 m × 80 m in the mining area. The diameter of the considered pillars varies between 4 m and 6 m. With continuous mining operations, the number of retained pillars in the mined-out stope has increased dramatically. The dip angle of the orebody is about 5 to 10 ° while the thickness of the orebody is about 0.5 m to 10 m. The grade of the orebody is evenly distributed with a mean grade of 0.35%. The 3D geological model of the mining operations is demonstrated in Fig. 1. One can also state that the orebody pillars have peeled off and the roof has collapsed with the continuous progress of mining production. During the mining activities, the roof above the mined-out area caves without causing any damage to mine structures and the overburden subsides in a controlled manner. Since premature caving can start hazardous roof falls while workers are present, pillar recovery has been less safe than other underground mining methods.

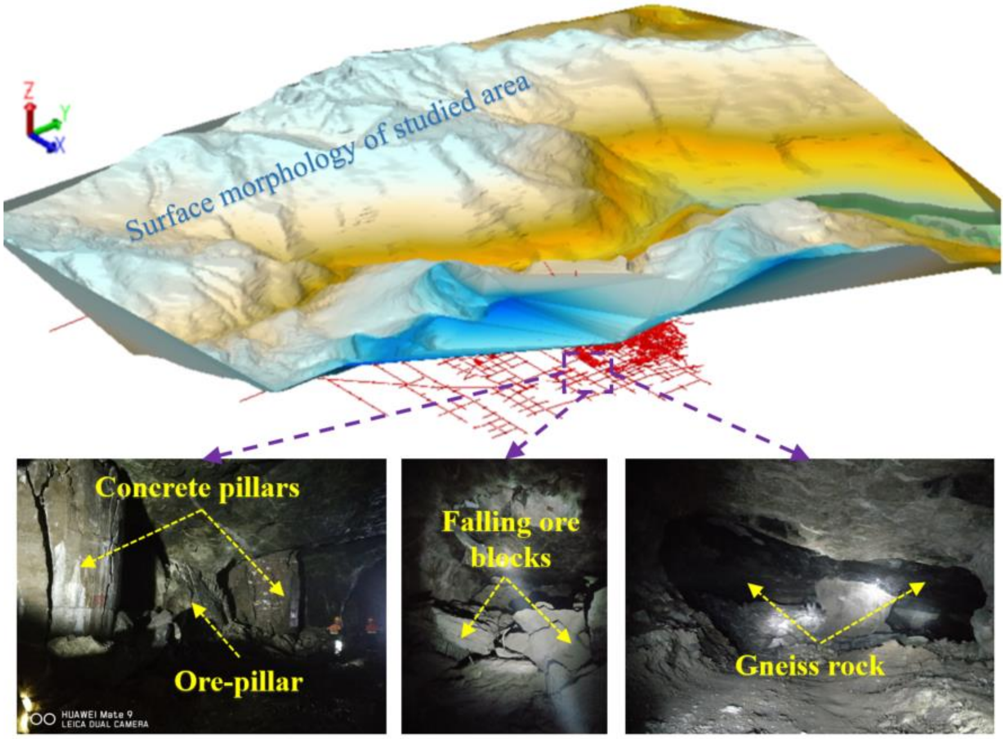

Fig. 1. The damage of orebody pillar in trial stope: morphology (top view); and concrete blocks (bottom view).

To mine the orebody pillars in the room-and-pillar mining method, as shown in Fig. 2, there are two replacement methods: artificial hydraulic prop (AHP) and fiber reinforced concrete (FRC). Fig. 2(a) displays the mining sequence of AHP. The AHP replacement method has been successfully applied in Chinese gypsum and bauxite mines. The main advantages of this method are high support strength and reusable application, low cost and large economic benefits. However, its application has limitations. The temporary support effect is poor when the height of the orebody pillar exceeding 4 m. Besides, the AHP recovery is directly operated under the roof and a relatively poor safety. The biggest disadvantage of this method is the lower recovery rate of the orebody pillars.

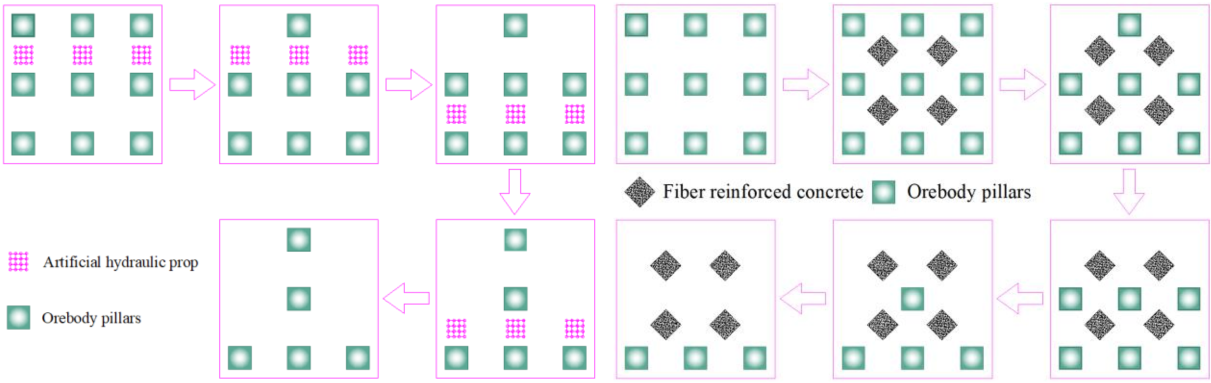

(a) Artificial hydraulic prop (AHP) (b) Fiber reinforced concrete (FRC)

Fig. 2. Two alternative types of pillar mining methods: (a) AHP, and (b) FRC.

Fig. 2(b) demonstrates the mining sequence of the FRC replacement method. The main advantages of this method are high pillar recovery rate, relatively simple construction and high safety. However, its disadvantage is that the intensity of workers is relatively large. After adding the fiber to concrete, it can increase its strength gain. The toughness of the concrete pillar is also increased, making pillar less likely to collapse and improving the safety of workers and equipment in the underground stopes.

2.2 Experimental materials

In this study, the fineness modulus of river sand was 2.5, and the particle size of gravel ranges from 5 mm to 12 mm. Researchers and engineers found that rubbers, fibers and other chemical materials can also well improve the mechanical strength properties of concrete. Fibers play a key role in the strength performance of concrete and have been widely utilized in the sprayed concrete support in tunneling and commercial construction building (Onuaguluchi and Banthia, 2019). Considering the exotherm of the hydration reaction and the corrosion resistance effect, glass, polypropylene (PP) and polyacrylonitrile (PAN) fibers, as shown in Figure 3, were selected as the main additive and reinforcement material in this study (Xue et al., 2018). Some basic parameters of the considered fiber types were listed in Table 1. The main chemical composition of Portland cement 42.5R is fully reported elsewhere (Cao et al. 2018). Note that the influence of tap water chemical composition on performance is ignored in this study.

Table 1 The fundamental mechanical parameters of the fiber types considered in this study

Fiber type	Length (mm)	Density (g/cm^3)	Tensile strength (MPa)	Elastic modulus (GPa)	Elongation rate (%)
Glass	12	2.02	369	4.89	36.5
PP	12	0.91	398	3.85	28
PAN	12	0.91	736	4.68	30

Fig. 3. Additive fibers used in the experiments: (a) glass fiber, (b) PP fiber, and (c) PAN fiber.

2.3 Specimen preparation

To explore the reasonable fiber content (FC), three types of FC values (0.4 wt.%, 0.8 wt.% and 1.2 wt.%) were utilized for preparing FRC samples. The non-fiber reinforced concrete (NFRC) sample was also prepared as a control sample for comparison. Since the original state of fibers was distributed in parallel bundles, they need to be separated sufficiently before FRC samples were manufactured. The river sand, gravels, ordinary Portland cement 42.5 R, fibers and tap water were thoroughly blended in a mixer for at least 5 min. The manufactured concrete slurries were gently poured into cylindrical molds having a diameter of 50 mm and a height of 100 mm. The specimens in the cylinders were then sealed to avoid water evaporation. The tested NFRC and FRC samples were then placed in the curing chamber which has a constant temperature of 20±1 °C and a relative humidity of 90±5%. Besides, it needs to be emphasized that the curing specimens are kept in the curing chamber for 14 days after cylindrical molds were removed after 48 hours. The curing chamber aimed to replicate in-situ curing conditions since samples are commonly surrounded by both underground hard rock masses and already-backfilled stopes, which cannot transfer heat exchange quickly.

2.4 Experimental methods

2.4.1 Uniaxial compressive strength test

To get the mechanical strength parameters of concrete, the uniaxial compressive strength (UCS) tests were conducted on laboratory-prepared samples after different curing times for the different studied fibers. Samples were tested by using a high-precision electronic universal testing machine to investigate the mechanical strength quality and performance of both NFRC and FRC samples. During the whole loading process, a constant displacement loading speed was set as 0.5 mm/min according to Chinese standard GB/T1767-1999 (Xue et al., 2019b; 2020; Cao et al., 2019a). Moreover, the axial deformations were automatically recorded by an electronic data acquisition system.

2.4.2 Computed tomography scanning test

The computed tomography (CT) system, based on the principle of X-ray radiation imaging, is a non-destructive test tool integrating nuclear technology, computer, control and precision machinery. The CT named IPT 61 (supplied from Granpect Company Limited) was used to investigate the interior pores and cracks in the tested FRC samples. The basic parameters considered were listed as follows: a spatial resolution of 2.5 LP/mm, a density resolution of 0.5 %, and an X-ray energy of 6 MeV. To better ensure the sample's integrity, the contact surface of the tested sample was wrapped with a transparent plastic film. The scanned data was recorded first and then stored to assist in subsequent reconstruction and analysis of the 3D model. Fig. 4 shows a flowchart of the methodology of the research implemented in this study, which consists mainly of three stages: Part 1 deals with macro-mechanical properties; Part 2 deals with micro-mechanical properties; and Part 3 deals orebody pillar stability calculations.

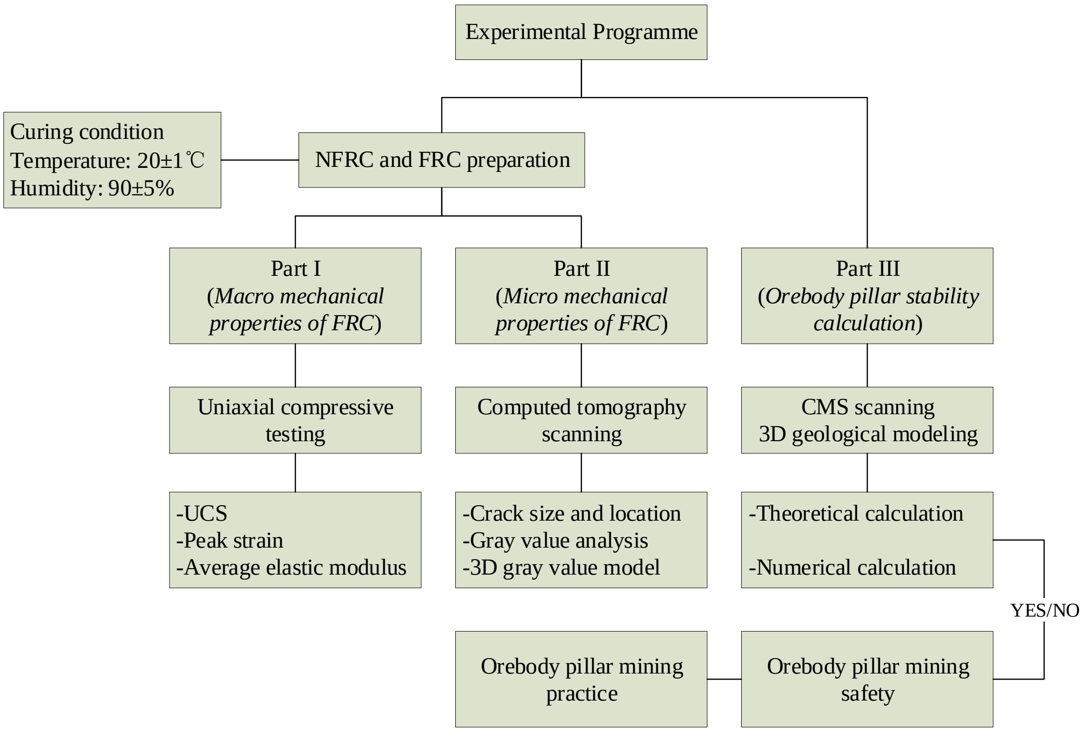

Fig. 4. A flowchart design of the methodology of the research implemented in this study.

3 Results and discussion

3.1 Stress-strain relationship for concrete samples

Fig. 5 shows the stress and strain curves of both NFRC and FRC samples, which is measured by the mechanical strength properties of cementitious materials. One can state that the whole stress and strain curves can be divided into four stages: i) porosity compaction stage; ii) linear elastic stage; iii) unsteady rupture stage; and iv) crack expansion stage, which have been explained by Cao et al (2019b; 2019c). In addition, the strength performance of the tested FRC samples with various fiber contents varied greatly.

The strength gains of NFRC samples quickly dropped after reaching their peak stresses. However, the stress of FRC samples gradually decreased after having enough strength and showed a good ductility. This means that fiber can limit the crack growth and hence improve the toughness of FRC samples.

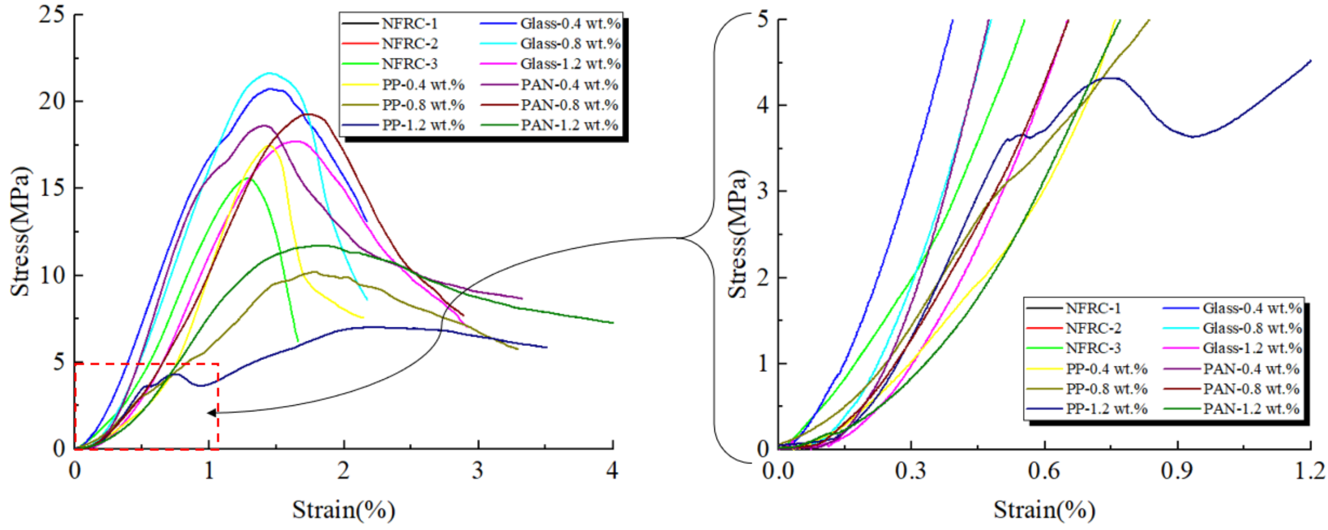

Fig. 5. Stress-strain relationship for NFRC and FRC: (a) loading whole process, and (b) initial loading stage.

As the compressive stresses of concrete increase, its elastic area becomes larger, and its load-bearing capacity reduces abruptly after the appearance of the maximum strength. The strengthening mechanism of fiber involves the transfer of stress from the matrix to the fiber by interlocking the fibers and matrices when the fiber surface is deformed. Hence, the stress is shared by the fibers and matrix in tension until the matrix cracks, and then the total stress is gradually transferred to the fibers. These characteristics of high-strength concrete are determined from the size of strain and the shape and rising and falling curves at the appearance of the maximum strength.

3.2 Effect of fiber content on compressive strength of concretes

Fig. 6 shows the histogram distributions of the compressive strengths of FRC and NFRC samples. To remove the errors caused by the laboratory tests, the effect of fiber content on strength performance of concrete samples was analyzed by averaging their UCSs. One can say that the compressive strength gain rises first and then reduces as the fiber content increases from 0 % to 1.2 %. The mean strength value of non-fiber reinforced concretes is 15.6 MPa. For a given fiber content of 0.4 wt.%, the strength values of glass, PP and PAN FRC samples are 20.6 MPa, 21.6 MPa and 18.6 MPa, respectively. The strength values of glass, PP and PAN FRC samples are 19.7 MPa, 20.8 MPa and 19.3 MPa when the fiber content is 0.8 wt.%. The strength values of glass, PP and PAN FRC samples containing a fiber content of 1.2 wt.% are 16.6 MPa, 17.7 MPa and 11.7 MPa, respectively. Besides, the corresponding strengths of glass and PP fiber reinforced concrete samples were larger than non-fiber reinforced ones, regardless of fiber content of 0.4 wt.%, 0.8 wt.% or 1.2 wt.%. However, the strengths of PAN FRC samples were 11.2 MPa when the fiber content is 1.2 %, which is fairly smaller than non-fiber reinforced concrete. The strength reduction rate of concretes continued to grow and reached 25 %.

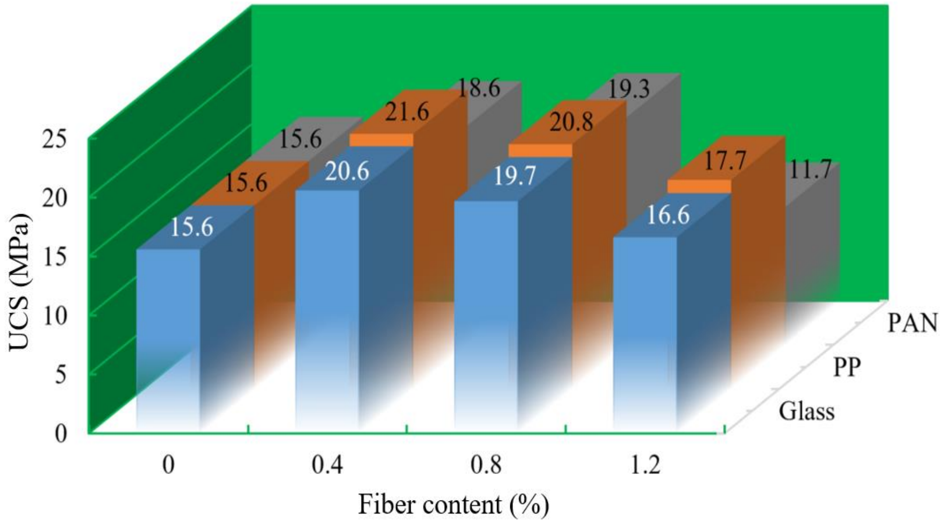

Fig. 6. The UCS histogram distributions of FRC and NFRC samples.

One can conclude that the rate of fiber addition plays a key role in the compressive strength of concretes. Adding the fibers to the concrete mix enhances the post-cracking response of the matrix and increases its toughness. When the fiber content increases in the mix, the hardened properties of concrete increases equivalently first and then decreases after reaching its optimum ratio. Different fiber addition rates lead to different shapes of the load-deflection curve. Among the three fibers studied, PP fiber is better than both glass and PAN fibers. This is because of the physical and mechanical properties of PP fiber which has a relatively high modulus of elasticity and rich bond. It is easy to obtain uniform dispersion with PP fibers when a sufficiently large volume of fibers is used in the matrix.

3.3 Effect of fiber content on peak strain of concrete samples

Fig. 7 shows the change in the peak strain of NFRC and FRC samples as a function of fiber content. PS, FC and R^2 were peak strain, fiber content and multiple correlation coefficient (MCC), respectively. To study the quantitative relationship between PS and fiber content, a total of four different functions: linear, exponential, logarithmic and power were used to fit their intrinsic properties. Note that the mean R^2 value of linear, exponential, logarithmic and power fitting were 0.9486, 0.9334, 0.8729 and 0.8965, respectively. In addition, one can also say that the linear correlation has the highest MCC. Consequently, the PS values of FRC samples increased linearly with increasing fiber content.

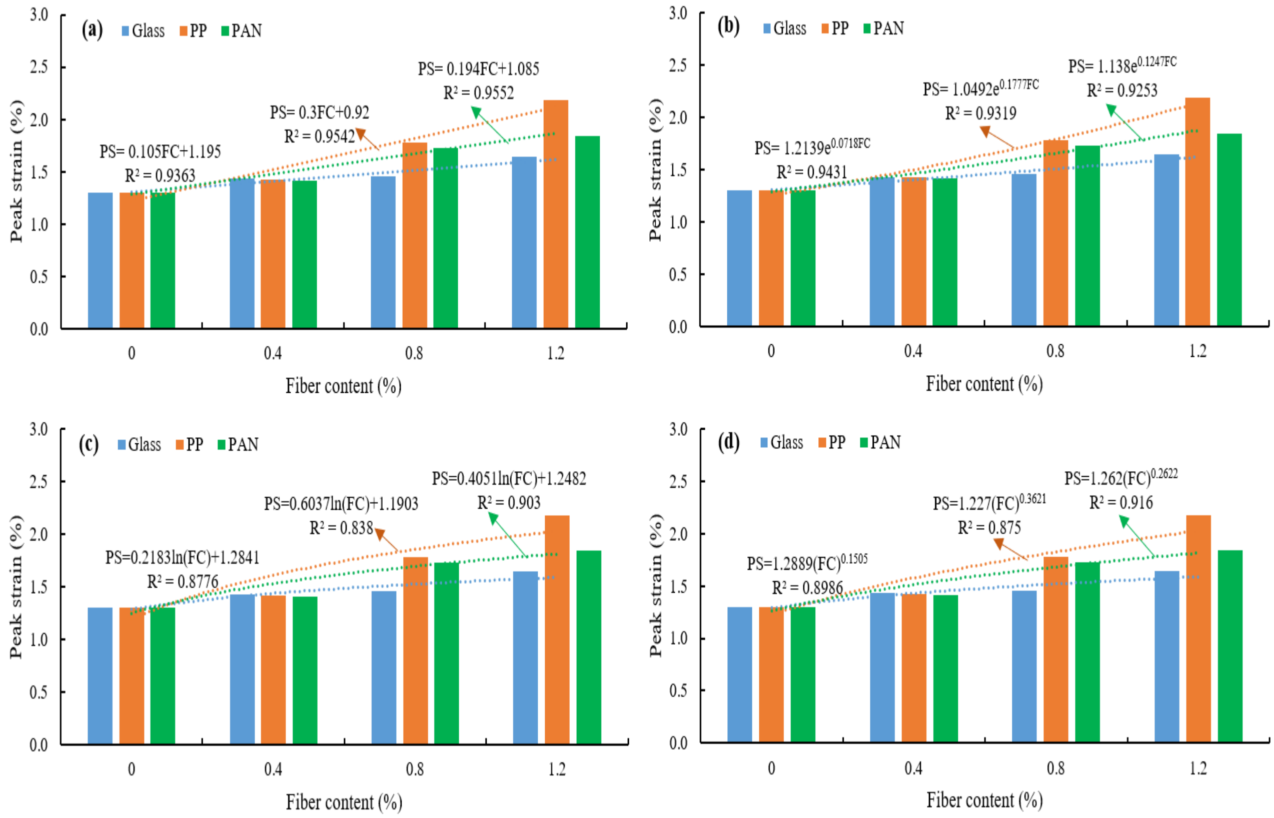

Fig. 7. Fitting results between peak strain and fiber content: (a) linear; (b) exponential, (c) logarithmic, (d) power.

The strain corresponding to the peak stress depends on the type of FRC samples with different fibers. The level of strain at peak stress decreases slowly with increasing deformations. This may be explained by the propagation of cracks generated in the pre-peak and peak. Once the opening of the formed crack increases, the stress-bearing capacity decreases significantly. When PP fibers with a high aspect ratio were mixed, the strain corresponding to the strength gain significantly increased with an increase in the fiber volumetric ratio. This tendency was not observed in the samples containing a fiber content of 0.4 wt.%, in which fibers with a low aspect ratio were mixed. The test results indicate that the strain at the compressive strength is affected by both the fiber volumetric ratio and fiber aspect ratio, which correspond to the number of fibers per unit concrete volume.

3.4 Effect of fiber content on elastic modulus of concrete samples

The results obtained from strength and peak strain studies show that PP fiber has obvious advantages than both PAN and glass fibers. Hence, this study finally has allowed us to pick the best fiber type as PP fiber. As stated by the stress-strain curves of PP FRC samples, the histogram between average elastic modulus (AEM) of PP FRC samples and fiber content was clearly shown in Fig. 8. One can say that the AEM values of PP FRC samples increase first and then decrease as the fiber content increases from 0 wt.% to 1.2 wt.%. The corresponding AEM values are 2125.78 MPa and 1301.19 MPa when the fiber content was 0.4 wt.% and 0.8 wt.%, respectively. Compared with NFRC samples, the growth rates of AEM were 91.2 % and 17.0 %, respectively. When the fiber content is 1.2 wt.%, the AEM values were smaller than those obtained from NFRC, and the reduction rate reached 70.7%.

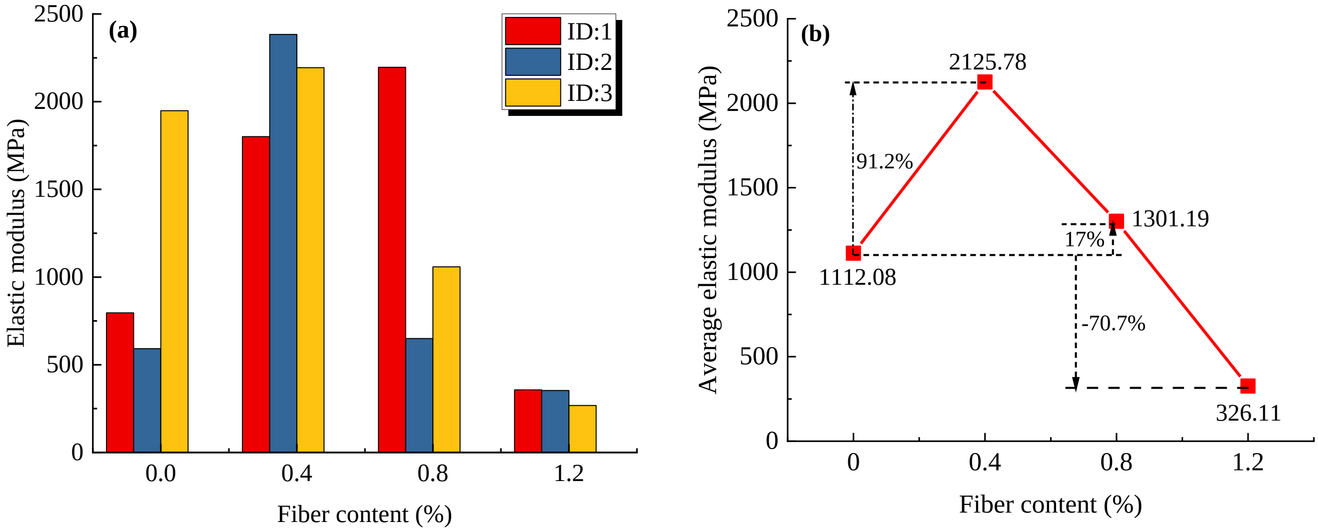

Fig. 8. Relationships for PP FRC and NFRC samples: (a) elastic modulus, and (b) average elastic modulus.

One can say that the elastic modulus of FRC increases up to a fiber content of 0.4 wt.% and then decreases with an increase in the fiber volumetric ratio (up to 1.2 wt.%). This enhancement is mainly due to the interlocking action of fibers, where fibers lock the large aggregate together in the matrix and stop the propagation and the opening of micro cracks, and thus inhibiting crack growth. The modulus of elasticity of FRC decreases as the fiber content increases to 1.2 wt.%. As a result, a similar sequence of reduction was also noticed for FRC samples present in the literature.

3.5 The mechanisms of fiber reinforced concrete

The main reason for adding fibers to the cementitious matrix is to enhance its fracture characteristics and structural behavior via the ability of fibers to bridge cracks (Fig. 9). This mechanism affects the serviceability and ultimate limit states. The effects on the service load behavior are typically controlled by crack propagation, which reduces the spacing and width of cracks. The effect on the behavior in the ultimate limit state is increased by the load resistance. Fibers also improve the stiffness and ductility of the cementitious matrix. Fig. 9 shows the bridging mechanism of FRC samples under uniaxial compression. The FRC matrix allows the cohesive-frictional resistance and fiber bridging effect between fibers and matrix. The combined actions lead to the brittle or ductile behavior of FRC and/or a transition zone from brittle to ductile, based on the used fiber content.

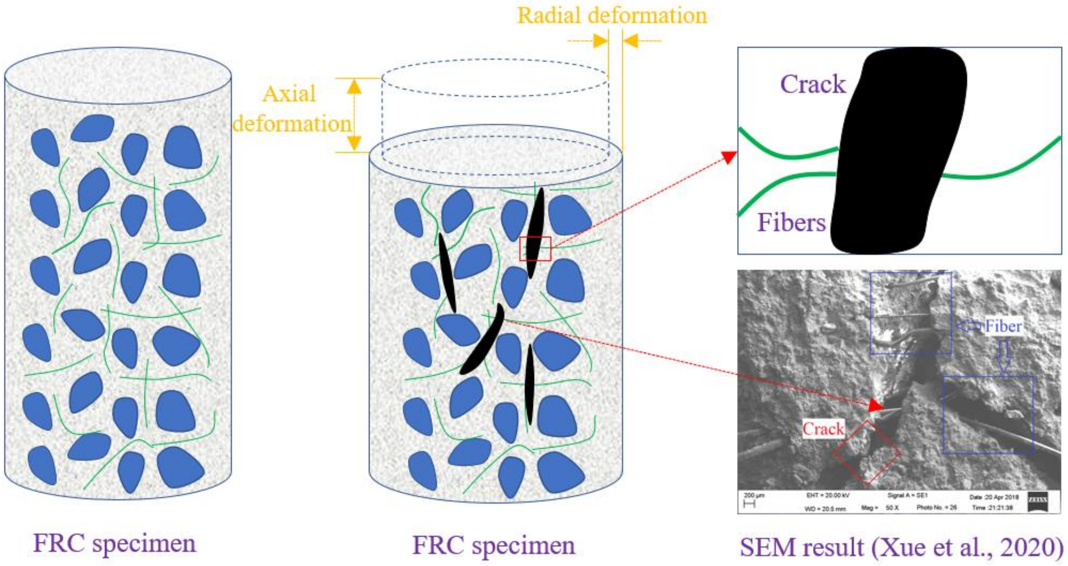

Fig. 9. Fiber bridging mechanism of fiber reinforced concrete under uniaxial compression.

When an external load is applied to the FRC matrix, the matrix will directly transfer some of the exerted loads to the fiber. Thus, before any cracks are initiated in the matrix, some of the external loads will be carried by fibers and the rest by the matrix. The volume and size of fibers in the matrix are important in reaching a substantial improvement in strength over corresponding mixtures without fibers. For most FRC matrix, the major reinforcing effect of fibers comes about first after matrix cracking. The failure mainly occurs because of fiber pull-out and fibers with deformed ends. A considerable energy dissipation takes place as the fiber is straightened and plastically deformed. Accordingly, unlike plain concrete, the FRC matrix does not break in such a brittle manner after the initiation of the first crack. This has the effect of increasing the work of fracture, which is referred to as toughness or fracture energy and is represented by the area under the stress-strain curve, as shown in Figure 5.

To improve the mechanical strength performance of the cementitious matrix, the chemical compositions of the matrix need to be characterized, well understood, and then improved. In Portland cement, the raw materials are limestone and clay. Therefore, a typical composition of ordinary Portland cement is about 67% calcium oxide and 22% silicon dioxide, with mainly alite and belite molecules. The products of the cement hydration reaction are portlandite and calcium silicate hydrate (C-S-H) gel. The C-S-H gel is up to 70% of the final volume in the cementitious matrix. The produced C-S-H gel from the hydration reaction is responsible for the cohesion and strong mechanical properties of the cementitious matrix. A total of three polymeric fibers, including polypropylene fiber were used to make the FRC matrix. Polypropylene fiber is typically composed of alkanes that have little intermolecular association since the carbon-hydrogen bond is nonpolar. Alkanes are typically nonpolar molecules and insoluble in water.

3.6 2D CT scanning characteristics analysis

Computed Tomography (CT) is an imaging technique where digital geometry processing can be used to generate a 3D-image of the brain's tissue and structures obtained from a large series of 2D X-ray images. CT scanning is an effective non-destructive test way, and the microstructure of cementitious materials can be well investigated by analyzing its internal pores and crack sizes (Sun et al., 2016; 2017). Fig. 10 shows the 2D CT cross-section of NFRC and PP FRC samples before and after loading. One can say that both NFRC and FRC samples have uneven pores distributed inside before compressive loadings. However, the 2D images after loading show that a large number of cracks are generated in the interior. In this study, Image J software was used to quantitatively analyze crack pore size and crack area ratio. It was also found that coarse aggregate and hydration products (C-S-H gels and C-H) have different colors within the matrix. The gray value 3D models were obtained by using the function named surface plot from analyzing module in Image J (Harris et al., 2018; Tang et al., 2010).

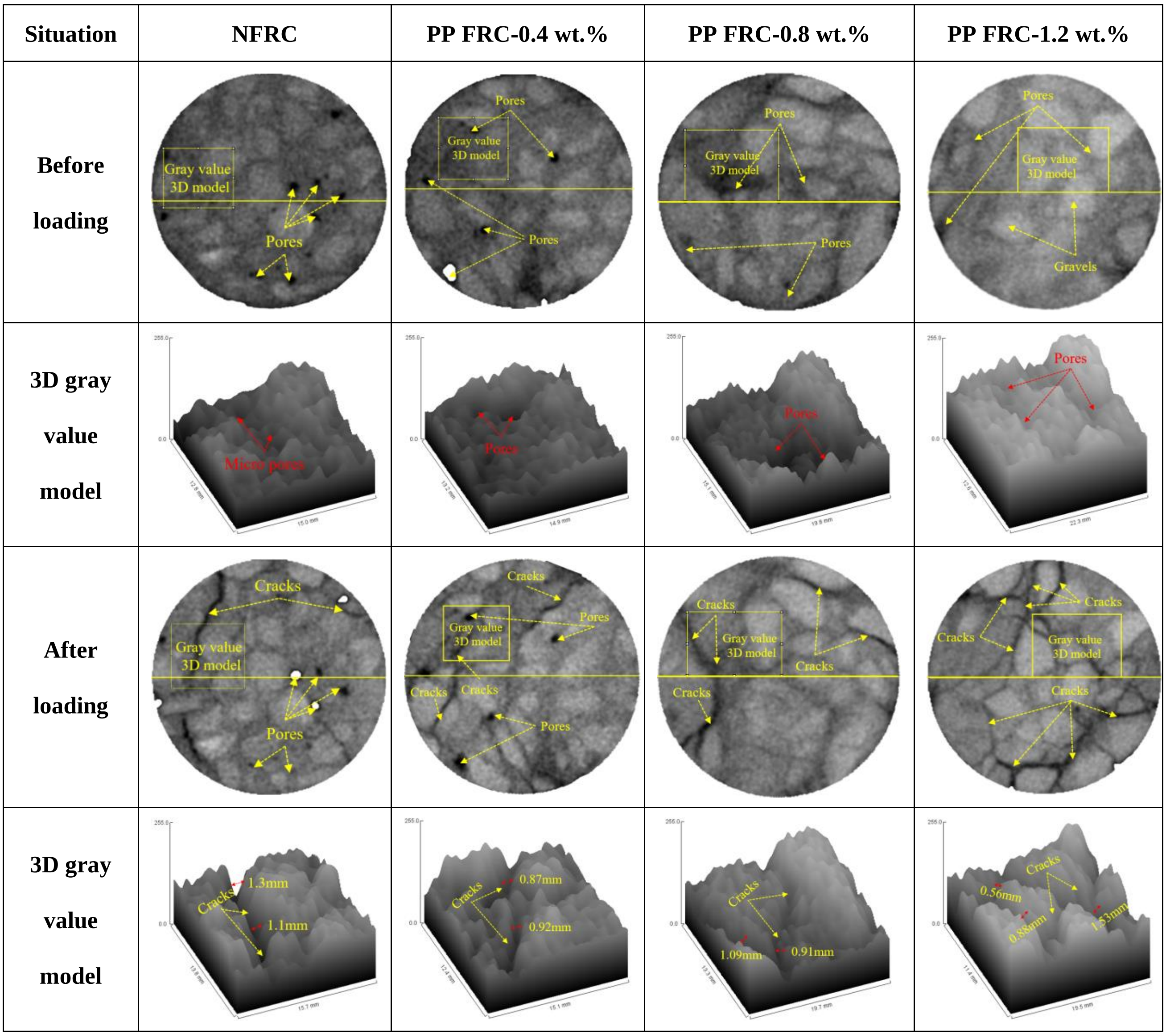

Fig. 10. 3D gray value model and 2D section scanning images of NFRC and FRC specimens.

Note that the darker the color, the smaller the gray value. Hence, the small gray value corresponds to the porosity before loading. Compared with the 3D models before loading, the gray value 3D models after loading can display the morphology and size of cracks. Laboratory tests show that a whole cutting crack near the boundary appears within NFRC after loading, and the maximum widths reached 1.3 mm. The five cracks appeared in the section of PP FRC-0.4 wt.% specimen. However, these cracks are not connected, and the maximum crack width was 0.92 mm. Besides, the cracks in the section of PP FRC-0.8 wt.% specimen also expanded, the crack size was small, and the maximum crack width was 1.09 mm. However, more cracks were generated in the section of PP FRC-1.2 wt.% sample. The cracks propagated along coarse aggregates, and cracks propagated along with the surface of coarse aggregates under the driving of external load. The maximum crack width reaches 1.53 mm. In this section, the set scale function was chosen to calibrate the specimen size in Fig. 10. Besides, the plot profile function was explored to extract the relationship between gray value and sample diameter. The relationship between gray value and distance before and after loading was also analyzed and shown in Fig. 11.

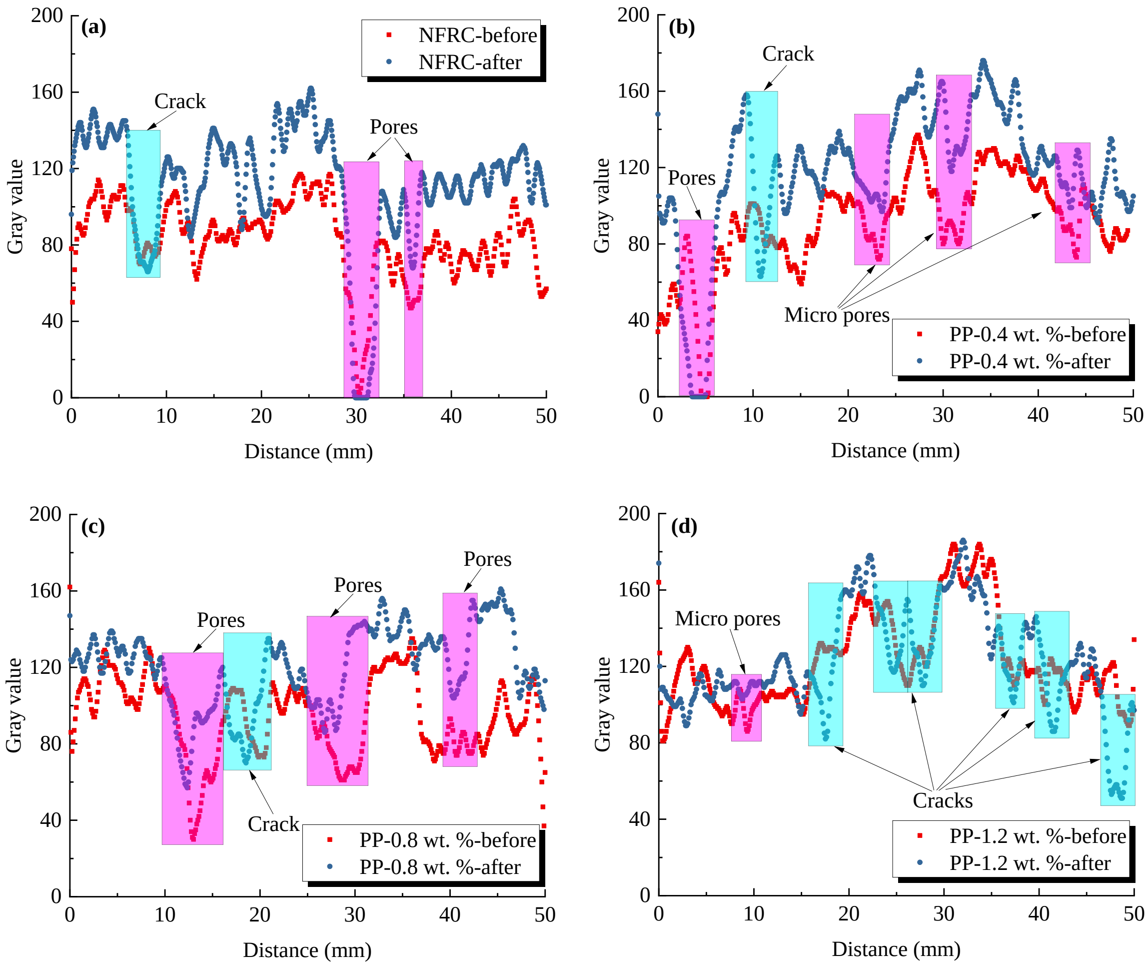

Fig. 11. Relationship between the intercept and the gray value before and after:

(a) NFRC, (b) PP-0.4 wt.%, (c) PP-0.8 wt.%, and (d) PP-1.2 wt.%.

The pores size, crack width and crack location are shown in Fig. 11. Fig. 11(a) shows that there are two pores at the 30 mm and 36 mm positions, and the main crack exists at the 8 mm position. One can also observe from Fig. 11(b) that there is one pore at the 5 mm position and there are three micropores at 23 mm, 31 mm and 44 mm positions, respectively. The main crack exists at the 12 mm position. Besides, Fig. 11(c) shows that three pores are distributed at 13 mm, 28 mm and 42 mm, respectively. The main crack exists in the 18 mm position. However, the results of Fig. 11(d) are different from the other results. There are nearly six cracks or micro-cracks existing in the section of PP FRC-1.2%. The gray distribution curves, as shown in Fig. 11, had a good correspondence with 2D CT pore and crack distribution. This means that the gray value processing can well characterize the microscopic structural characteristics of both NFRC and FRC samples.

4 Orebody pillars mining practice

4.1 Pillars accurate 3D modeling

The implementation of CMS, supplied from Geosight Inc., was used for scanning the mined-out area and orebody pillars in the trial stope. Some parameters were explained as follows: a field of view of 360 ° × 300 °, and a scanning angle of 0.5 °, 1 ° and 2 °, respectively. When a set scan angle was small, more point cloud data was acquired, and the models of established pillars were more accurate. The scanning distance was up to 500 m, and the accuracy of distance measurement and distance resolution were ±2 cm and 1 mm, respectively. Other parameters included: scanning speed was 250 points/second, and the average scanning time was 7 min. Its weight was 7.2 kg and the data transmission could be wired or wireless. The data output format is DXF, XYZ coordinates, etc., and the operating temperature is -30 °C ~ +60 °C. Fig. 12 shows a flowchart of orebody pillar stability analysis.

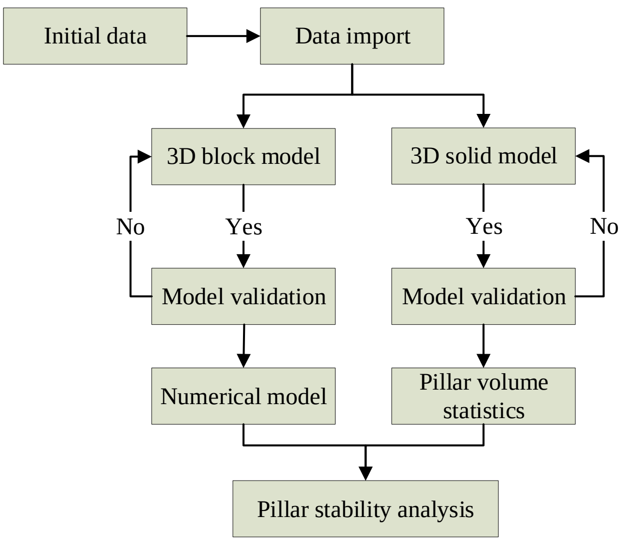

Fig. 12. Flowchart of orebody pillar stability analysis.

The stability analysis of the orebody pillar which is undertaken by the use of any of the traditional methods is started by excavation as the first step. Then, concrete pillars are designed by considering the mode of possible failures and economic constraints. If concrete pillars are deemed as a viable option then the design process, as shown in Fig. 12, can be applied by dealing with the determination of the stresses caused by the unstable zone. A proper diameter and the number of concrete pillars required for the stability of underground mines is chosen. Note that the design of concrete pillars should be checked if it is stable, operationally feasible and economically competitive.

Fig. 13 shows the schematic diagrams of the multi-point scanning of cylindrical pillars. Because the actual shape of orebody pillars is cylindrical, laser scanning cannot obtain all the point cloud data of the pillar outlines at one shot. Therefore, for each single orebody pillar, at least two or three test points for scanning is chosen by a proper angle (120 °) of scanning points, as shown in Fig. 13(a). Then, the point cloud obtained is subjected to a series of processing such as Boolean operation, cutting and division. Then all 3D geological models of orebody pillars are obtained.

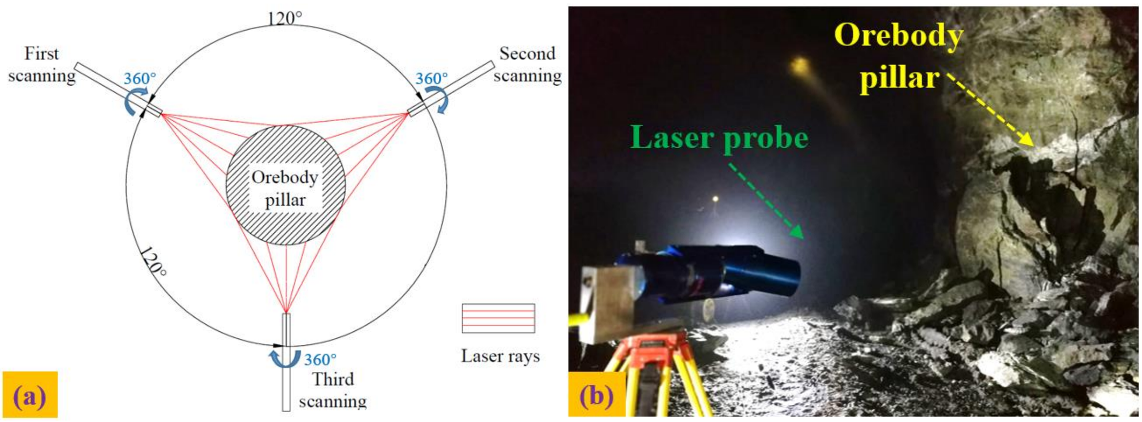

Fig. 13. Multi-point scanning of cylindrical pillars: (a) schematic diagram, and (b) monitoring of orebody pillar.

It is important to have some redundancy to check for blunders and to improve the precision of scanning. Note that averaging repeat scan clouds give better precision than single-point precision. In general, the design should establish a network of reference points with a geodetic network designed near the object being monitored in the underground structures.

4.1.1 3D models of ordinary concrete pillars

The point data obtained from Geosight CMS equipment was imported into the 3D mine modeling software, and the 3D solid model of the mined-out areas and pillars are obtained through functions such as editing, deleting and splicing. The solid model of ordinary concrete pillars was shown in Fig. 14.

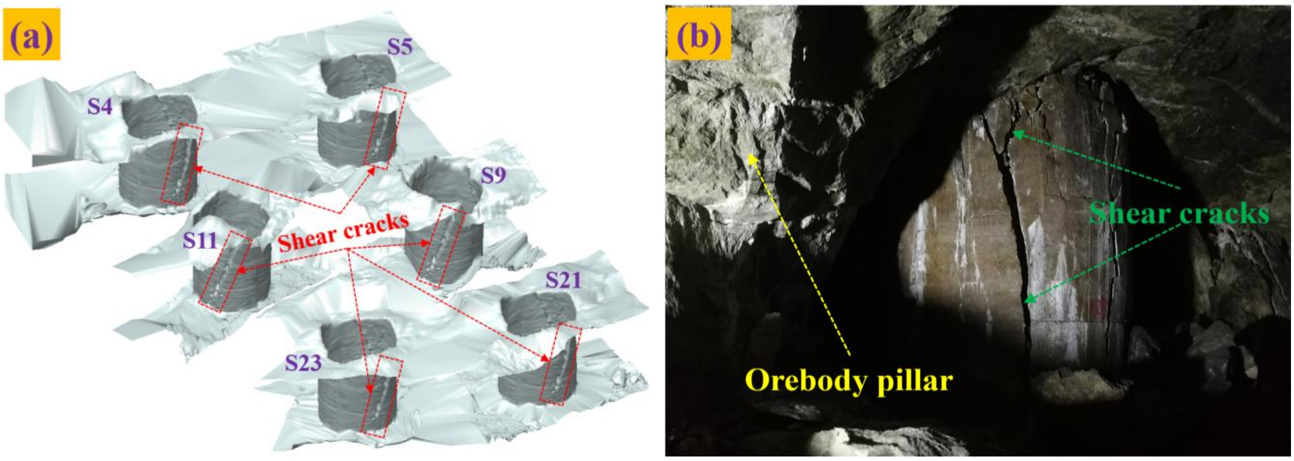

Fig. 14. Schematic diagrams of multi-point scanning of cylindrical pillars: (a) location of working pillars, and (b) orebody pillar and crack formations.

Cracking in reinforced concrete pillar is a serious problem and it may lead to the loss of strength, stability and durability. Therefore, it is required to investigate different types of cracks that may initiate in the pillar to consider suitable means to restrict them. Overall, one can state that there are one or more cracks on the surface of concrete pillars. The failure modes of pillars are induced by shear cracks. Moreover, field works indicate that concrete pillars are easy to fall off, and the safety risks of orebody pillars mining were so high.

4.1.2 3D models of orebody pillars

Fig. 15 shows a 3D geological model of both mined-out areas and pillars. In this study, the prepared mining orebody pillars were S12, S13, S14, S15, S18, S19, S20, S22, S24 and S26, respectively. The accurate volume of the orebody pillar is obtained through 3D solid modeling. The weight of orebody pillars in the trial stope has been obtained by considering an ore density of 3.1 t/m^3. A summary of the results obtained from the modeling is listed in Table 3.

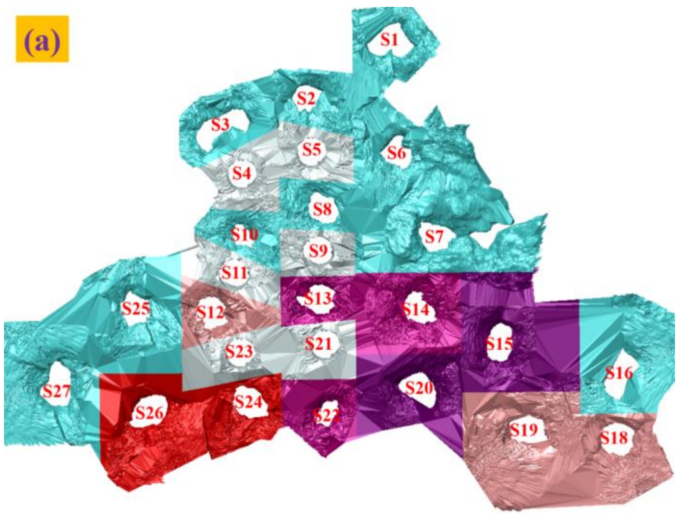

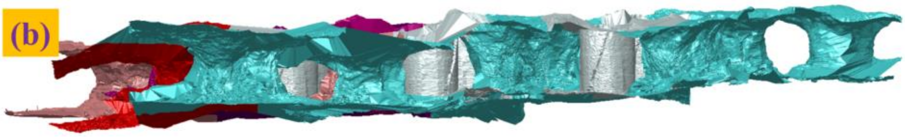

Fig. 15. The 3D geological modeling of the mined-out area and pillars: (a) main view, and (b) side view.

Table 3 Basic information of orebody pillars in trial stope

Pillar No.	Height (m)	Grade (%)	Volume (m^3)	Weight (t)	Pillar No.	Height (m)	Grade (%)	Volume (m^3)	Weight (t)
S12	6.5	0.4	144.56	448.15	S19	6.6	0.5	140.60	435.86
S13	7.3	1.2	131.33	407.13	S20	7.1	2.0	137.74	426.99
S14	7.4	1.2	181.48	562.59	S22	6.8	1.2	75.52	234.12
S15	5.5	1.5	145.94	452.41	S24	6.9	0.8	118.10	366.10
S18	6.5	0.4	176.00	545.60	S26	7.0	0.8	144.93	449.29
Sum			1396.21	4328.24					

One can observe that the overall grade of the pillars in the trial stopes is high, the grade distribution varies from 0.4% to 2.0%, and the weight of pillar varies between 234 tons and 563 tons. The trial stope has 10 pillars with a total ore weight of 4238.24 tons. Note that rigorous grade and mining quality control during stoping can reduce dilution. Thus, the model considered for the stability design needs to be constantly upgraded as the operations develop and lessons learned.

4.2 Stability calculation of orebody pillars

The stability and strength performance of concrete pillars is evaluated by calculating the safety factor. The distribution of pillars is irregular in the trial stope. Hence, the Voronoi diagram method was used to theoretically calculate the stability of concrete pillars. The empirical formula (e.g., Hedley and Grant, Von Kinmmelmann and Potvin and Sjoberg) for the strength performance of hard rock pillars was used for calculating the safety factor for each tested pillar (Xu et al., 2015; Song et al., 2014).

According to the factors affecting the stability of concrete pillars, based on the safety factor method of pillar, only the influencing factors that can be quantitatively analyzed were considered in this study. The calculation formula of the safety factor of concrete pillar could be derived as follows:

$$F_s = \left(133 \frac{W^{0.5}}{h^{0.75}}\right) \Big/ \left(\gamma H \, S_v / S_p\right) \qquad (1)$$

$$F_s = \left(65\frac{W^{0.46}}{h^{0.66}}\right) \Big/ \left(\gamma H\, S_v / S_p\right) \tag{2}$$

$$F_s = \left(0.42\sigma_c \frac{W}{h}\right) \Big/ \left(\gamma H\, S_v / S_p\right) \tag{3}$$

$$F_s = \left[74\left(0.778 + 0.222\frac{w}{h}\right)\right] \Big/ \left(\gamma H\, S_v / S_p\right) \tag{4}$$

where F_s is the safety factor of the concrete pillar; σ_c is the uniaxial compressive strength (MPa); γ is the density of overburden rock mass (t/m^3); H is the buried depth of concrete pillar (m); w is the width of the concrete pillar (m); h is the height of concrete pillar (m). S_v is the section area of the Voronoi diagram (m^2); S_p is the section area of the concrete pillar (m^2).

Fig. 16 shows the relationship between the orebody pillar and the safety factor. If the long-term stability of the pillar is not considered, that is, only the stability during the production of the orebody pillar is considered, and other support measures are not taken. It is recommended that the safety factor F_s of the considered concrete pillars is 1.0 when the pillar is static mining. The average safety factor values of the considered ten pillars were generally larger than 1.0. Accordingly, one can consider that all of these orebody pillars can be mined safely.

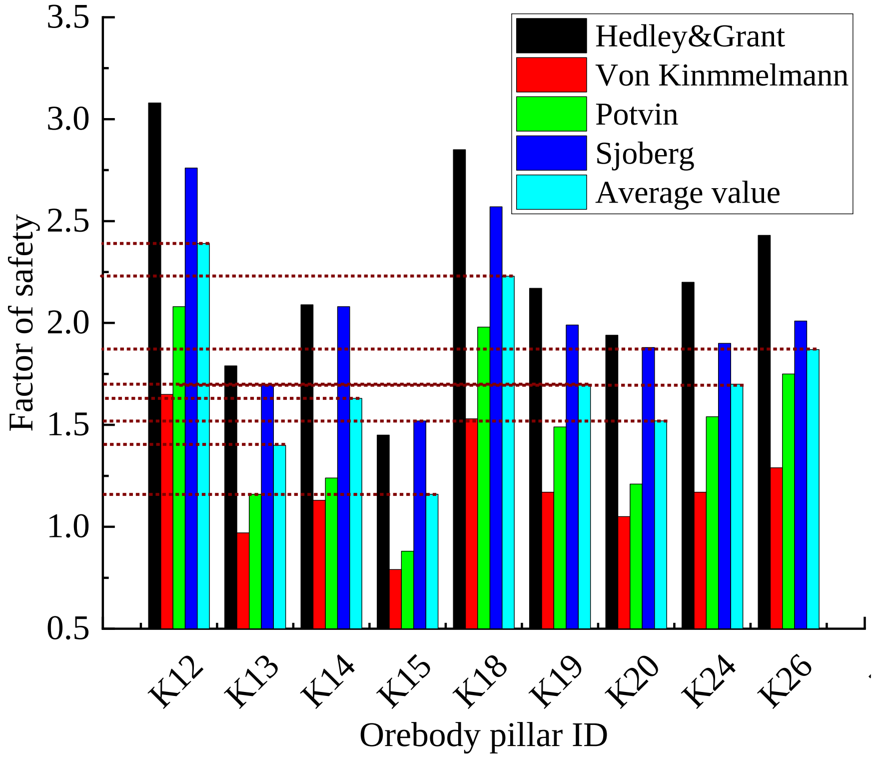

Fig. 16. Relation between orebody pillar ID and safety factor.

6.3 Stability numerical simulation of orebody pillars

6.3.1 Numerical model building

The number of index parameters such as elastic modulus, tensile strength, cohesion, internal friction angle, unit volume weight, and Poisson ratio was also determined for rock samples received from the NM. A summary of the obtained results is listed in Table 4. To analysis the pillar strength changes in the trial stopes during ore excavation, FLAC^{3D} was used for numerical simulation. For all the analyses, the Hoek-Brown strength criterion was considered. The numerical simulation area of the trial stope is in X direction: 41211.688 to 41279.786, the model width is 108 m, the Y direction is: 65724.652 to 65818.259, the model length is 134 m, and the mesh size in the X and Y directions is 1 m; The height of the column is 1196.507 to 1201.707, the height of the top and bottom plates is 30 m, the height of the model is 75 m, and the grid size in the Z direction is 0.5 m.

Table 4 Some mechanical properties of the rocks considered in this study

Mechanical parameters	Roof	Orebody	Foot
Elastic modulus (GPa)	7.512	18.672	23.792
Tensile strength (MPa)	2.0	2.2	1.5
Cohesion (MPa)	3.71	10.296	11.362
Internal friction angle (º)	30.25	33.52	41.74
Unit volume weight (t/m^3)	2.78	3.17	2.62
Poisson ratio	0.227	0.233	0.245

Due to the small size of the pillar, the grid size of 1 m × 1 m × 0.5 m cannot be achieved. The exact division of the pillar model, therefore, the sub-classification of the blocks constituting the pillar, that is, the size of the block is optimized, and the size of the block is selected by 0.5 m × 0.5 m × 0.2 m. The simulated model is clearly shown in Fig. 17. Note that ‘Diban’ stands for the floor; ‘dingban’ stands for trial stope roof; ‘dpwkz’ stands for low-grade pillar; ‘kongqu’ stands for goaf; ‘s12’ means pillar, ‘weiyan’ stands for surrounding rock; and ‘ysjz’ stands for originally artificial concrete pillar. Concerns were raised about the stress regime around the pillars because of the complex orebody interaction and the extent of previous stoping within the area. Therefore, numerical modeling was conducted using a 3-D boundary element code to predict the likely stress levels and to determine the size of the pillars to be left between the panel stopes. Two design criteria were used to assess the numerical result predictions. Firstly, the max. principle stress should not exceed a critical value of 40 MPa. Secondly, an extension strain should not exceed a critical value of 150 μs if the considered pillar was to be stable.

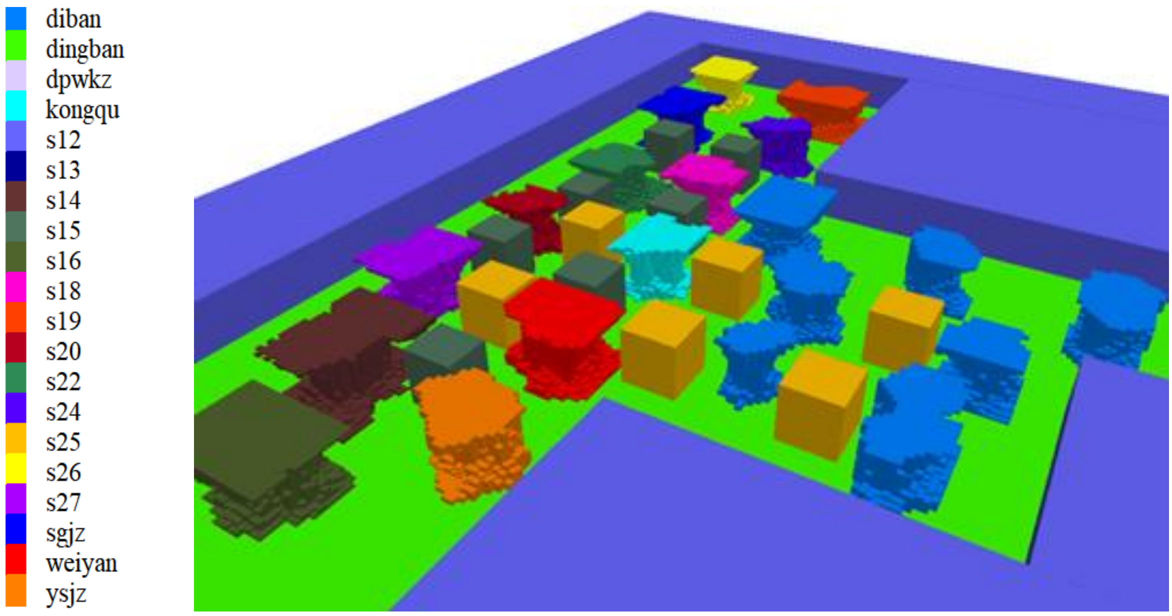

Fig. 17. Numerical model of pillars in trial stope.

6.3.2 Pillar design of fiber reinforce concrete

For the model with a coordinate (28, 75 and 37.5) as the origin, the vertical Y-axis profile is obtained, and the vertical stress distribution at each position in the point column can be obtained. The calculation results are clearly shown in Fig. 18 and Fig. 19. Generally, one can observe from Fig. 18 that the maximum vertical stress within the pillar is 25 MPa before pillars excavation. The maximum vertical displacement in the roof is 14.2 mm. Additionally, it can be seen from Fig. 19 that there is a slight subsidence in the roof of the stope and the amount of roof subsidence is relatively large within the exposed area of the roof. The bottom plate has a slight bulge. The maximum bulging amount is 6.5 mm, and the displacements in the top plate and the bottom plate are both small, indicating that the top and bottom plates are relatively safe. It can be seen from the distribution of the plastic zone that the roof plate is less likely to fall, and the roof is stable.

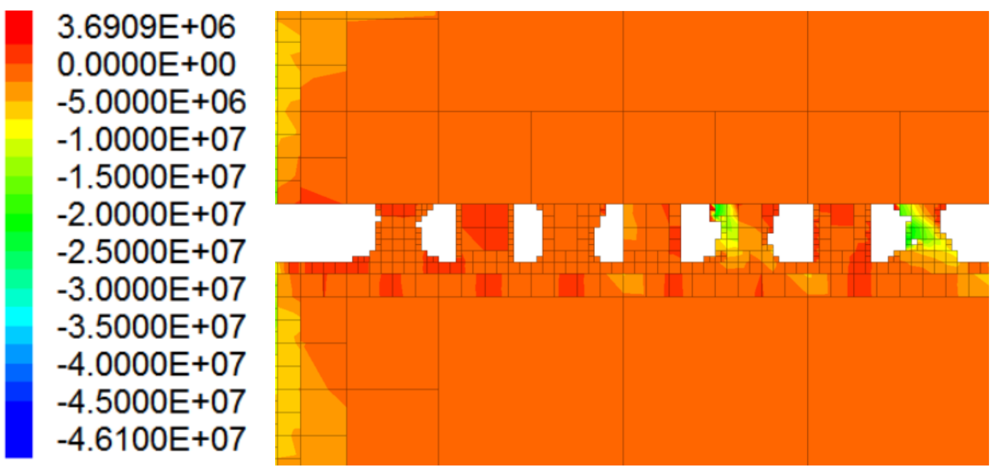

Fig. 18. Vertical stress distribution in pillars.

Fig. 19. Vertical displacement distribution in pillars.

4.4 Pillar mining industrial test in trial stope

4.4.1 Orebody pillars mining process in trial stope

Fig. 20 shows the orebody pillars mining in the trial stope. In this study, the selected orebody pillars in the trial stope were distributed between line 6 and line 4. The thickness of the orebody varies between 5 m and 8 m. The geomorphology of the mining area was hilly, and the rock characteristics of roof, orebody and floor were gneiss, skarn and gneiss, respectively. Likewise, the burial depth of the orebody is uneven, and the burial depth varies between 100 m and 1500 m. Additionally, Fig. 20 shows the pillar mining process in the NM. Initially, a separate borehole is designed for each pillar by using 3DMINE software. Then the borehole location on-site is placed. After blasting, the collapsed ore is quickly discharged and transported. Finally, the mined-out area is treated by using the brick wall.

The mining process is indeed differentiated from other open-stoping methods, in that the support rock typically extends from hanging wall to footwall in the form of pillars. Pillars are usually round or rectangular and are surrounded by open excavations called rooms. In the room and pillar mining, engineers have a choice of whether to take the whole orebody in one slice or multiple slices. The need for multiple slices can arise when the orebody is very thick, and the pillars cannot support the full height of the deposit. Multi-pass mining is used in mines where there is uncertainty in stress conditions and the engineer decides to take a more cautious first pass and determine from there what the best course of action would be. In hard-rock mines, it is often too difficult to verify the exact thickness of a deposit because of poor continuity. When this is the case, it is difficult to decide between single and multi-pass room and pillar and it is typically recommended to begin on the projected topmost slice to make it easy for the back to be reached.

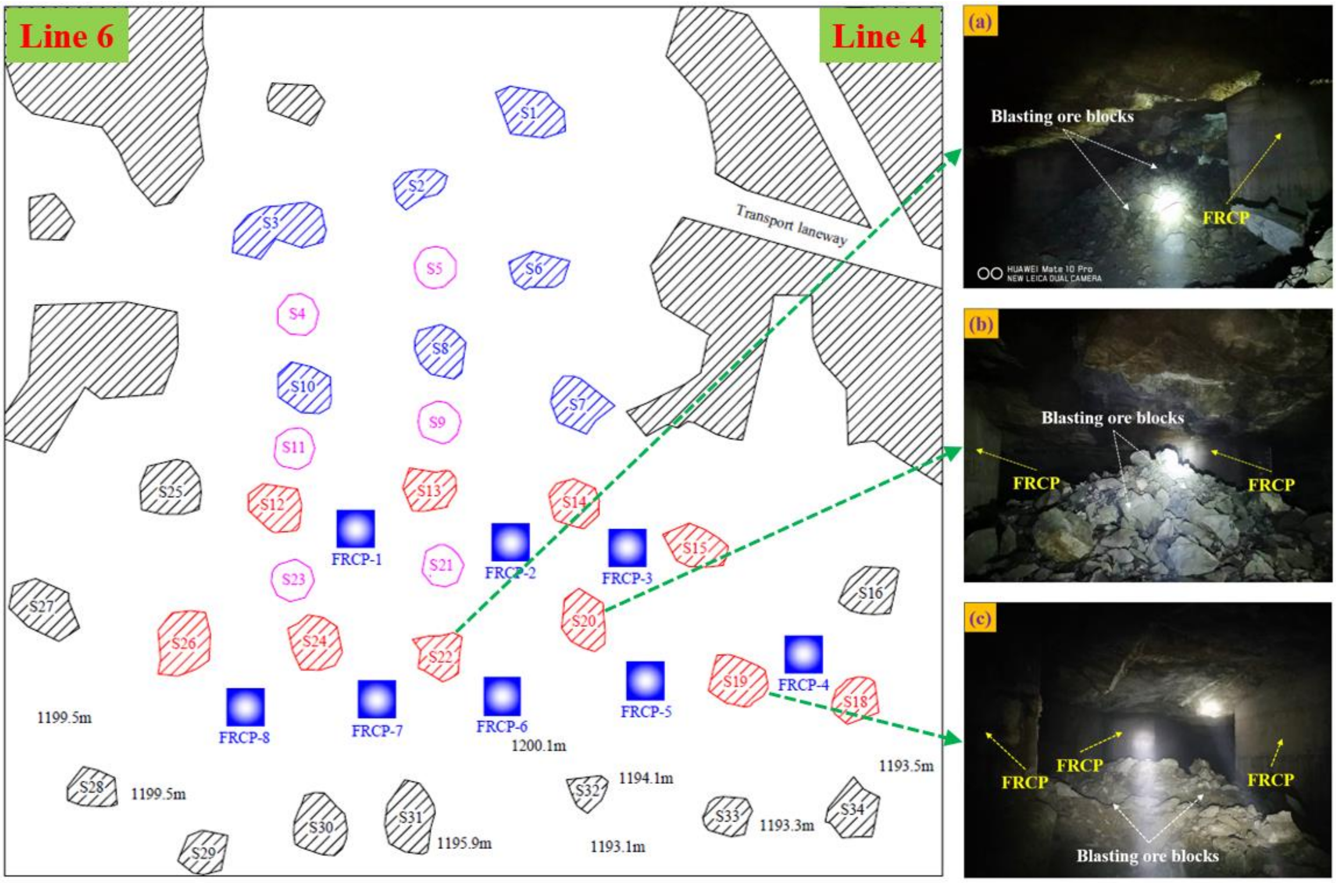

Fig. 20. Pillar mining in trial stope: (a) S19; (b) S20; and (c) S22.

5 Conclusions

In this study, fiber reinforced concrete was considered as artificial pillar for extracting the orebody pillars. Some techniques such as uniaxial compressive strength test and industrial computed tomography scanning test were used for investigating the macro- and micro-mechanical properties of concrete pillars. A cavity monitoring system was chosen for rebuilding the accurate 3D modeling to measure the total weight of pillars. The theoretical calculation and numerical simulation were adopted for studying the stability of orebody pillars. From the performed tests, the following conclusions can be drawn.

The strength values increased first and then decreased as the fiber content in the matrix increased from 0 wt.% to 1.2 wt.%. The peak strain values of FRC increased linearly with increasing fiber content. The gray distribution curve had a good correspondence with the two-dimensional CT pore and crack distribution. The numerical results showed that the vertical stress and plastic zone were small when pillars were mined out. It meant that the location and size of concrete pillars were suitable in the trial stope. Both theoretical analysis and numerical results showed that the pillars could be fully recovered safely, and the mining of the pillars in the test stope had achieved good economic benefits.

This study shows that the concrete pillar is a powerful means in designing pillars of underground mines to safely extract the ore. Thanks to this new technique, the amount of the recovered ore from the stopes can be increased safely and efficiently by considering the pillar loading capacity, pillar stiffness, and neighboring rock stability. The practical outcome of the model may assist in the understanding of the stability of underground mines and assessing the safety of pillar recovery. It can be also considered as an initial valuation of safe pillar sizing, where no pillar failures and risks can take place. It is thought that replacing the ore left underground with concrete pillars will make vital contributions to short- and long-term mining operations. The proposed methodology can be used to provide preliminary design specifications. However, it should be kept in mind that there is a nonstop risk linked with underground mining operations mainly due to the natural variability of underground conditions and structures. As more data on operational and quality control considerations become available, mines will modify their designs in a safer mode. At present, there are still a number of works that need to further investigate. These are the field monitoring of concrete pillars as a function of stress and depthless; use of concrete pillars for metalliferous, non-metalliferous and coal mines; a study of microstructural and geotechnical properties of concrete pillars; and industrial application and promotion of orebody pillar mining. These considerations are the foremost subjects of on-going research by the authors.

CRediT author statement

Shuai Cao: Conceptualization, Methodology, Formal analysis, Writing-Review and Original Draft. **GaiLi Xue:** Investigation, Methodology, Visualization, Writing-Review and Editing. **Erol Yilmaz:** Validation, Methodology, Visualization, Writing-Review and Editing. **ZhenYu Yin:** Visualization, Writing-Review and Editing. **FuDou Yang:** Visualization, Writing-Review and Editing.

Acknowledgments

This work was financially supported by the National Natural Science Foundation of China (grant numbers: 51804017 and 51974012), the Open Fund of the Key Laboratory of Ministry of Education for Efficient Mining and Safety of Metal Mines (grant number: USTBMSLAB201804) and Fundamental Research Funds for Central Universities (Grant No. FRF-TP-20-001A2 and FRF-BD-19-005A).

Conflicts of interest

The authors declare that the work described has not been published before; that it is not under consideration for publication anywhere else; that its publication has been approved by all co-authors; that there is no conflict of interest regarding the publication of this article.

References

Aarthi, K., Arunachalam, K., 2018. Durability studies on fibre reinforced self-compacting concrete with sustainable wastes. J. Clean. Prod. 174, 247-255. https://doi.org/10.1016/j.jclepro.2017.10.270

Alp, I. Deveci, H., Sungun, Y.H., Yilmaz, A.O., Kesimal, A., Yilmaz, E., 2009. Pozzolanic characteristics of a natural raw material for use in blended cements. Iran. J. Sci. Tech. Transac. B: Eng. 33(4), 291-300. https://doi.org/10.22099/IJSTC.2009.707

Bdulkareem, M., Havukainen, J., Horttanainen, M., 2019. How environmentally sustainable are fibre reinforced alkali-activated concretes? J. Clean. Prod. 236, 117601. https://doi.org/10.1016/j.jclepro.2019.07.076

Buttignol, T.E.T., 2019. A load induced thermal strain (LITS) semi-empirical model for plain and steel fiber reinforced concrete subjected to uniaxial compressive load. Cem. Concr. Res. 127, 105896. https://doi.org/10.1016/j.cemconres.2019.105896

Botín, J.A., Vergara, M.A., 2015. A cost management model for economic sustainability and continuous improvement of mining operations. Resour. Pol. 46(2), 212-218. https://doi.org/10.1016/j.resourpol.2015.10.004

Cao, S., Yilmaz, E., Song, W.D., 2018. Dynamic response of cement-tailings matrix composites under SHPB compression load. Constr. Build. Mater. 186, 892-903. https://doi.org/10.1016/j.conbuildmat.2018.08.009

Cao, S., Yilmaz, E., Xue, G.L., Yilmaz, E., Song, W., 2019a. Loading rate effect on uniaxial compressive strength behavior and acoustic emission properties of cemented tailings backfill, Constr. Build. Mater. 213, 313-324. https://doi.org/10.1016/j.conbuildmat.2019.04.082

Cao, S., Yilmaz, E., Song, W.D., 2019b. Fiber type effect on strength, toughness and microstructure of early age cemented tailings backfill. Constr. Build. Mater. 223, 44-54. https://doi.org/10.1016/j.conbuildmat.2019.06.221

Cao, S., Yilmaz, E., Xue, G.L., Song, W.D., 2019c. Assessment of acoustic emission and triaxial mechanical properties of rock-cemented tailings matrix composites. Adv. Mater. Sci. Eng. 6742392. https://doi.org/10.1155/2019/6742392

Cao, S., Zheng, D., Yilmaz, E., Yin, Z.Y., Xue, G.L., Yang, F.D., 2020. Strength development and microstructure characteristics of artificial concrete pillar considering fiber type and content effects. Constr. Build. Mater. 256, 119408. https://doi.org/10.1016/j.conbuildmat.2020.119408

Chan, R., Santana, M.A., Oda, A.M., Paniguel, R.C., Vieira, L.B., Figueiredo, A.D., Galobardes, I., 2019. Analysis of potential use of fibre reinforced recycled aggregate concrete for sustainable pavements. J. Clean. Prod. 218, 183-191. https://doi.org/10.1016/j.jclepro.2019.01.221

Chen, M., Zhong, H., Zhang, M.Z., 2020. Flexural fatigue behavior of recycled type polymer fibre reinforced concrete. Cem. Concr. Compos. 105, 103441. https://doi.org/10.1016/j.cemconcomp.2019.103441

Consoli, N.C., Marques, S.F.V., Sampa, N.C., Bortolotto, M.S., Siacara, A.T. Nierwinski, H.P., Pereira, F., Festugato, L., 2017. A general relationship to estimate strength of fibre-reinforced cemented fine-grained soils. Geosynth. Int. 24(4), 435-441.

Deng, J., Kanwar, N.S., Pandey, M.D., Xie, W.C., 2019. Dynamic buckling mechanism of pillar rockbursts induced by stress waves. J. Rock. Mech. Geotech. Eng. 11, 944-953. https://doi.org/10.1016/j.jrmge.2019.02.005

Dong, L., Tong, X., Li, X., Zhou, J., Wang, S., Liu, B., 2019. Some developments and new insights of environmental problems and deep mining strategy for cleaner production in mines. J. Clean. Prod. 210, 1562-1578. https://doi.org/10.1016/j.jclepro.2018.10.291.

Esterhuizen, G.S., Dolinar, D.R., Ellenberger, J.L., 2011. Pillar strength in underground stone mines in the United States. Int. J. Rock Mech. Min. Sci. 48, 42-50. https://doi.org/10.1016/j.ijrmms.2010.06.003

Emeka, A.E., Chukwuemeka, A.J., Okwudili, M.B., 2018. Deformation behaviour of erodible soil stabilized with cement and quarry dust. Emerg. Sci. J. 2, 383-387. https://doi.org/10.28991/esj-2018-01157

Facconi, L., Minelli, F., 2020. Behavior of lightly reinforced fiber reinforced concrete panels under pure shear loading. Eng. Struct. 202, 109879. https://doi.org/10.1016/j.engstruct.2019.109879

Feo, L., Ascione, F., Penna, R., Lau, D., Lamberti, M., 2020. An experimental investigation on freezing and thawing durability of high-performance fiber reinforced concrete (HPFRC). Compos. Struct. 234, 111673. https://doi.org/10.1016/j.engstruct.2019.109879

Ghasemi, E., Ataei, M., Shahriar, K., 2014. An intelligent approach to predict pillar sizing in designing room and pillar coal mines. Int. J. Rock Mech. Min. Sci. 65, 86-95. https://doi.org/10.1016/j.ijrmms.2013.11.009

Ghasemi, E., Shahriar, K., Sharifzadeh, M., 2010. A new method for risk assessment of pillar recovery operation. Safety Sci. 48, 1304-1312. https://doi.org/10.1016/j.ssci.2010.04.008

Grzymski, F., Musiał, M., Trapko, T., 2019. Mechanical properties of fibre reinforced concrete with recycled fibres. Constr. Build. Mater. 198, 323-331. https://doi.org/10.1016/j.conbuildmat.2018.11.183

Harris, C., Alcock, A., Trefan, L., Nuttall, D., Evans, S.T., Maguire, S., Kemp, A.M., 2018. Optimising the measurement of bruises in children across conventional and cross polarized images using segmentation analysis techniques in Image J, Photoshop and circle diameter measurements. J. Fore. Leg. Med. 54, 114-120. https://doi.org/10.1016/j.jflm.2017.12.020

Hauquin, T., Deck, O., Gunzburger, Y., 2016. Average vertical stress on irregular elastic pillars estimated by a function of the relative extraction ratio. Int. J. Rock Mech. Min. Sci. 83, 122-134. https://doi.org/10.1016/j.ijrmms.2015.12.004

Hesami, S., Hikouei, I.S., Emadi, S.A.A., 2016. Mechanical behavior of self-compacting concrete pavements incorporating recycled tire rubber crumb and reinforced with polypropylene fiber. J. Clean. Prod. 133, 228-234.

https://doi.org/10.1016/j.jclepro.2016.04.079

Jiang, H.Q., Yi, H., Yilmaz, E., Liu, S., Qiu, J., 2020. Ultrasonic evaluation of strength properties of cemented paste backfill: Effects of mineral admixture and curing temperature. Ultrasonics, 100, 105983. https://doi.org/10.1016/j.ultras.2019.105983

Kadam, S.S., Karjinni, V.V., Jarali, C.S., 2019. Prediction of fiber reinforced concrete strength properties by micromechanics method. Civ. Eng. J. 5, 200-208. https://dx.doi.org/10.28991/cej-2-19-03091238

Kaliyavaradhan, S.K., Ling, T.-C., Mo, K.H., 2020. Valorization of waste powders from cement-concrete life cycle: A pathway to circular future. J. Clean. Prod. 268, 122358. https://doi.org/10.1016/j.jclepro.2020.122358

Koohestani, B., Darban, A.K., Mokhtari, P., Yilmaz, E., Darezereshki, E., 2019. Comparison of different natural fibers treatments – A literature review. Int. J. Env. Sci. Tech. 16, 629-642. https://doi.org/10.1007/s13762-018-1890-9

Laurence, D., 2011. Establishing a sustainable mining operation: an overview. J. Clean. Prod. 19, 278-284. https://doi.org/10.1016/j.jclepro.2010.08.019

Li, L.C., Tang, C.A., Wang, S.Y., Yu, J., 2013. A coupled thermo-hydrologic-mechanical damage model and associated application in a stability analysis on a rock pillar. Tunn. Undergr. Sp. Tech. 34, 38-53. https://doi.org/10.1016/j.tust.2012.10.003

Li, M., Zhang, J., Li, A., Zhou, N., 2020. Reutilization of coal gangue and fly ash as underground backfill materials for surface subsidence control. J. Clean. Prod. 254, 120113.

Li, Y.H., Li, K.M., Feng, X.T., Cai, M., 2018. Development and evaluation of artificial expandable pillars for hard rock mining. Int. J. Rock Mech. Min. Sci. 110, 68-75. https://doi.org/10.1016/j.ijrmms.2018.07.014

Liu, J.L., Jia, Y.M., Wang, J., 2019. Calculation of chloride ion diffusion in glass and polypropylene fiber-reinforced concrete. Constr. Build. Mater. 215, 875-885. https://doi.org/10.1016/j.conbuildmat.2019.04.246

Lu, H., Qi, C.C., Li, C.H., Gan, D., Du, Y., Li, S., 2020. A light barricade for tailings recycling as cemented paste backfill. J. Clean. Prod. 247, 119388. https://doi.org/10.1016/j.jclepro.2019.119388

Malli, T., Yetkin, M.E., Ozfırat, M.K., Kahraman, B., 2017. Numerical analysis of underground space and pillar design in metalliferous mine. J. Afr. Earth. Sci. 134, 365-372. https://doi.org/10.1016/j.jafrearsci.2017.07.018

Merli, R., Preziosi, M., Acampora, A., Lucchetti, M.C., Petrucci, E., 2020. Recycled fibers in reinforced concrete: A systematic literature review. J. Clean. Prod. 248, 119207. https://doi.org/10.1016/j.jclepro.2019.119207

Mo, J.X., Zeng, L., Liu, Y.H., Ma, L.L., Liu, C.J. Xiang, S., Cheng, G.Y., 2020. Mechanical properties and damping capacity of polypropylene fiber reinforced concrete modified by rubber powder. Constr. Build. Mater. 242, 118111. https://doi.org/10.1016/j.conbuildmat.2020.118111

Mawat, H.Q., Ismael, M.Q., 2020. Assessment of moisture susceptibility for asphalt mixtures modified by carbon fibers. Civ. Eng. J. 6, 304-317. http://dx.doi.org/10.28991/cej-2020-03091472

Napa-García, G.P., Câmara, T.R., Torres, V.P.N., 2019. Optimization of room-and-pillar dimensions using automated numerical models. Int. J. Min. Sci. Tech. 29, 797-801. https://doi.org/10.1016/j.ijmst.2019.02.003

Onuaguluchi, O., Banthia, N., 2019. Value-added reuse of scrap tire polymeric fibers in cement-based structural applications. J. Clean. Prod. 231, 543-555. https://doi.org/10.1016/j.jclepro.2019.05.225

Qin, Y., Zhang, X.W., Chai, J.R., Xu, Z.G., Li, S.Y., 2019. Experimental study of compressive behavior of polypropylene-fiber-reinforced and polypropylene-fiber-fabric-reinforced concrete. Constr. Build. Mater. 194, 216-225. https://doi.org/10.1016/j.conbuildmat.2018.11.042

Qiu, R.J., Lin, M., Ruan, J.J., Fu, Y.G., Hu, J.Q., Deng, M.L., Tang, Y.T., Qiu, R.L., 2020. Recovering full metallic resources from waste printed circuit boards: A refined review. J. Clean. Prod. 244, 118690. https://doi.org/10.1016/j.jclepro.2019.118690

Renani, H.R., Martin, C.D., 2018. Modeling the progressive failure of hard rock pillars. Tunn. Undergr. Sp. Tech. 74, 71-81. https://doi.org/10.1016/j.tust.2018.01.006

Seccatore, J., Marin, T., De Tomi, G., Veiga, M., 2014. A practical approach for the management of resources and reserves in small-scale mining. J. Clean. Prod. 84, 803-808. https://doi.org/10.1016/j.jclepro.2013.09.031

Sherizadeh, T., Kulatilake, P.H.S.W., 2016. Assessment of roof stability in a room and pillar coal mine in the U.S. using three-dimensional distinct element method. Tunn. Undergr. Sp. Tech. 59, 24-37. https://doi.org/10.1016/j.tust.2016.06.005

Signorini, C., Sola, A., Malchiodi, B., Nobili, A., Gatto, A., 2020. Failure mechanism of silica coated polypropylene fibres for fibre reinforced concrete (FRC). Constr. Build. Mater. 236, 117549. https://doi.org/10.1016/j.conbuildmat.2019.117549

Song, W.D., Cao, S., Fu, J.X., Jiang, G.J., Wu, F., 2014. Sensitivity analysis of impact factors of pillars stability and its application. Rock Soil Mech. 35(1), 271-277. https://doi.org/10.16285/j.rsm.2014.s1.033

Sun, Q., Zhang, J.X., Zhou, N., 2018. Study and discussion of short-strip coal pillar recovery with cemented paste backfill. Int. J. Rock Mech. Min. Sci. 104, 147-155. https://doi.org/10.1016/j.ijrmms.2018.01.031

Sun, W., Hou, K.P., Yang, Z.Q., Wen, Y.M., 2017. X-ray CT three-dimensional reconstruction and discrete element analysis of the cement paste backfill pore structure under uniaxial compression. Constr. Build. Mater. 138, 69-78. https://doi.org/10.1016/j.conbuildmat.2017.01.088

Sun, W., Wu, A.X., Hou, K.P., Yang, Y., Liu, L., Wen, Y.M., 2016. Real-time observation of meso-fracture process in backfill body during mine subsidence using X-ray CT under uniaxial compressive conditions. Constr. Build. Mater. 113, 153-162. https://doi.org/10.1016/j.conbuildmat.2016.03.050

Salim, L.G., Al-Baghdadi, H.M., Muteb, H.H., 2019. Reactive powder concrete with steel, glass and polypropylene fibers as a repair material. 5, 2441-2449. https://dx.doi.org/10.28991/cej-2019-03091422

Tang, X.N., Berman, A.E., Swanson, R.A., Yenari, M.A., 2010. Digitally quantifying cerebral hemorrhage using Photoshop® and Image J. J. Neurosci. Meth. 190, 240-243. https://doi.org/10.1016/j.jneumeth.2010.05.004

Tesarik, D.R., Seymour, J.B., Yanske, T.R., 2009. Long-term stability of a backfilled room and pillar test section at Buick Mine, Missouri, USA. Int. J. Rock Mech. Min. Sci. 46, 1182-1196. https://doi.org/10.1016/j.ijrmms.2008.11.010

Usman, M., Farooq, S.H., Umair, M., Hanif, A., 2020. Axial compressive behavior of confined steel fiber reinforced high strength concrete. Constr. Build. Mater. 230, 117043. https://doi.org/10.1016/j.conbuildmat.2019.117043

Waclawik, P., Snuparek, R., Kukutsch, R., 2017. Rock bolting at the room and pillar method at great depth. Procedia Eng. 191, 575-582. https://doi.org/10.1016/j.proeng.2017.05.220

Wang, J.Q., Dai, Q.L., Si, R.Z., Guo, S.C., 2019. Mechanical, durability, and microstructural properties of macro synthetic polypropylene (PP) fiber-reinforced rubber concrete. J. Clean. Prod. 234, 1351-1364. https://doi.org/10.1016/j.jclepro.2019.06.272

Wang, P., Gao, N., Ji, K., Stewart, L., Arson, C. DEM analysis on the role of aggregates on concrete strength. Comput Geotech, 2020, 119, 103290. https://doi.org/10.1016/j.compgeo.2019.103290.

Xu, W.B., Song, W.D., Cao, S., Jiang, G.J., Wu, F., Jiang, L., 2015. Stope stability in underground mine and its control technique. J. Min. Safety Eng. 32(4), 658-664. https://doi.org/10.13545/j.cnki.jmse.2015.04.022

Xu, S., Suorineni, F.T., An, L., Li, Y.H., Jin, C.Y., 2019. Use of an artificial crown pillar in transition from open pit to undergrdoun mining. Int. J. Rock. Mech. Min. Sci. 117, 118-131. https://doi.org/10.1016/j.ijrmms.2019.03.028

Xue, G.L., Yilmaz, E., Song, W.D., Cao, S., 2018. Compressive strength characteristics of cemented tailings backfill with alkali-activated slag. Appl. Sci. 8, 1537. https://doi.org/10.3390/app8091537

Xue, G.L., Yilmaz, E., Song, W.D., Cao, S., 2019a. Mechanical, flexural and microstructural properties of cement-tailings matrix composites: Effects of fiber type and dosage. Compos. Part B: Eng. 172, 131-142. https://doi.org/10.1016/j.compositesb.2019.05.039

Xue, G.L., Yilmaz, E., Song, W.D., Yilmaz, E., 2019b. Influence of fiber reinforcement on mechanical behavior and microstructural properties of cemented tailings backfill. Constr. Build. Mater. 213, 275-285. https://doi.org/10.1016/j.conbuildmat.2019.04.080

Xue, G.L., Yilmaz, E., Song, W.D., Cao, S., 2020. Fiber length effect on strength properties of polypropylene fiber reinforced cemented tailings backfill specimens with different sizes. Constr. Build. Mater. 241, 118113. https://doi.org/10.1016/j.conbuildmat.2020.118113

Xiong, B.B., Demartino, C., Xiao, Y., 2019. High-strain rate compressive behavior of CFRP confined concrete: Large diameter SHPB tests. Constr. Build. Mater. 201, 484-501. https://doi.org/10.1016/j.conbuildmat.2018.12.144

Yilmaz, E., Belem, T., Benzaazoua, M., 2013. Study of physico-chemical and mechanical characteristics of consolidated and unconsolidated cemented paste backfills. Miner. Resour. Manag. 29(1), 81-100.

https://doi.org/10.2478/gospo-2013-0006

Yin, S., Shao, Y., Wu, A., Wang, H., Liu, X., Wang, Y., 2020. A systematic review of paste technology in metal mines for cleaner production in China. J. Clean. Prod. 247, 119590

Yu, Y., Deng, K., Luo, Y., Chen, S.E., Zhuang, H.F., 2018. An improved method for long-term stability evaluation of mining and pillar design. Int. J. Rock Mech. Min. Sci. 105, 98-109. https://doi.org/10.1016/j.ijrmms.2018.04.04<5

Zingano, A., Weiss, A., 2019. Subsidence over room and pillar retreat mining in a low coal seam. Int. J. Min. Sci. Tech. 29(1), 51-57. https://doi.org/10.1016/j.ijmst.2018.11.022